Fast ion confinement during high power tangential neutral beam injection into low plasma current discharges on the ISX-B tokamak

1988 Nucl. Fusion 28 951

(http://iopscience.iop.org/0029-5515/28/6/001)

FAST ION CONFINEMENT DURING HIGH POWER TANGENTIAL NEUTRAL BEAM INJECTION INTO LOW PLASMA CURRENT DISCHARGES ON THE ISX-B TOKAMAK

A. CARNEVALI*, S.D. SCOTT**, H. NEILSON,
M. GALLOWAY, P. STEVENS+, C.E. THOMAS++
Oak Ridge National Laboratory,
Oak Ridge, Tennessee,
United States of America

ABSTRACT. The beam ion thermalization process during tangential neutral beam injection in the ISX-B tokamak is investigated. The classical model is tested in co- and counter-injected discharges at low plasma current, a regime where large orbit width excursions enhance the importance of the loss regions. To test the model, experimental charge exchange spectra are compared with the predictions of an orbit following Monte Carlo code. Measurements of beam-plasma neutron emission and measured decay rates of the emission following beam turnoff provide additional information. Good agreement is found between theory and experiment. Furthermore, beam additivity experiments show that, globally, the confinement of beam ions remains classical, independently of the injected beam power. However, some experimental evidence suggests that the fast ion density in the plasma core did not increase with beam power in a way consistent with classical processes.

1. INTRODUCTION

Neutral beam injection has proved to be an effective means of providing auxiliary heating for tokamak plasmas. A record high ion temperature of 20 keV has been obtained on the Tokamak Fusion Test Reactor, TFTR [1], and a volume averaged $\langle\beta_T\rangle$ near 5% has been attained on Doublet-III [2] and on the Princeton Beta Experiment, PBX [3]. Early experiments — characterized by injected beam powers P_b comparable with or smaller than the Ohmic input power P_{OH} — indicated that the fast ion behaviour is classical. These experiments were the Oak Ridge Tokamak, ORMAK [4], the Adiabatic Toroidal Compressor, ATC [5], the British experiment, CLEO [6], and the Russian T-11 [7]. Subsequently, as higher beam power levels were achieved, scaling results incorporating data from a number of different tokamaks showed that the global energy confinement time τ_E^* decreases as P_b is increased [8]. To ensure that this decrease in τ_E^* with P_b is not a consequence of overestimating the beam power delivered to the plasma, it is necessary to ascertain that the beam ion thermalization process is well understood. High power injection experiments on several tokamaks have generally indicated that the beam ions behave classically. These experiments were the Impurity Study Experiment, ISX-B [9], the Princeton Large Torus, PLT [10, 11], the Tokamak Fontenay-aux-Roses, TFR [12], and the Poloidal Divertor Experiment, PDX [13]. However, anomalous fast ion losses have been reported in some cases, most notably on the PDX, in the presence of the magnetohydrodynamic (MHD) activity (fishbone instability) that accompanies the high power, near-perpendicular injection at high values of $q\langle\beta_t\rangle$ [14, 15]. Since the ISX-B, with quasi-tangential injection, was typically operated at lower I_p values than other high power tokamak experiments (e.g. PLT), this paper extends the investigation of fast ion confinement into a regime where large width orbit effects are expected to be significant. Emphasis is placed on systematic comparisons of discharges with low (I_p = 100 kA) and relatively high (I_p = 180 kA) plasma currents, for both co- and counter-injection. Experimentally measured energy spectra of charge exchange beam neutrals escaping from the plasma are compared with

* Present address: Rensselaer Polytechnic Institute, Troy, NY 12180, USA.
** Present address: Princeton Plasma Physics Laboratory, Princeton, NJ 08544, USA.
+ Permanent address: University of Tennessee at Knoxville, Nuclear Engineering Department, Knoxville, TN 37916, USA.
++ Present address: Georgia Institute of Technology, Nuclear Engineering Department, Atlanta, GA 30332, USA.

the calculated spectra. This is a particularly sensitive test of the theory because it reflects local values of beam and plasma parameters, as opposed to power transfer calculations, in which integral quantities are considered. Calculations of the power delivered to the plasma in the high and low I_p cases as estimated by an orbit following Monte Carlo code are also presented. Additional information is provided by neutron emission measurements and beam additivity experiments. Recent results from TFR [16], with quasi-perpendicular neutral beam injection, show that the beam ion density in the central region of the plasma appears to saturate with injected power. A similar indication of non-additivity of the central fast ion density was observed in ISX-B [17] and is described here.

Section 2 briefly reviews the experimental configuration and the methods used for the investigation. In Section 3, experimental data are compared with the predictions of classical theory. Conclusions are drawn in Section 4.

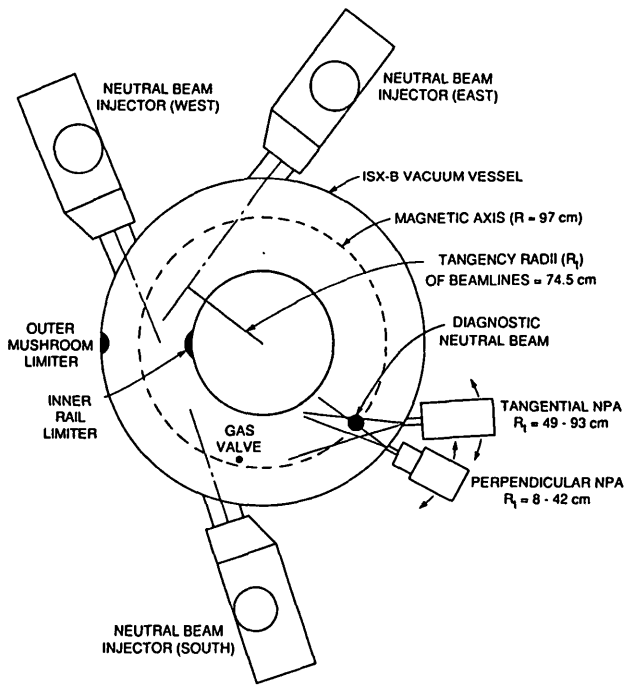

FIG. 1. Layout of the ISX-B experiment. The relative locations of the tangential neutral beam injectors and the horizontally scanning neutral particle analysers (NPAs) are shown. A diagnostic neutral beam was injected vertically close to the plasma centre. The limiters straddled the horizontal midplane.

2. EXPERIMENTAL CONFIGURATION AND METHODS

2.1. Configuration

Figure 1 shows a plan view of the ISX-B tokamak (R_0 = 93 cm, a = 27 cm) and the relative locations of the three neutral beam injectors (H^0, R_t = 74.5 cm) and the two neutral particle analysers (NPAs). Details of the machine parameters, objectives and confinement results are reviewed elsewhere [9, 18–21]. Fast ion data were collected in D^+ discharges run with an outer mushroom limiter and an inner rail limiter, both made of TiC coated graphite. Except for some of the beam–plasma neutron emission measurements, all the discharges discussed here were gettered with titanium. This does not present a limitation since it has been shown that the fast ion behaviour in gettered and ungettered discharges is similar [17]. Two mass discriminating neutral particle analysers, the Momentum Energy Analyser (MEA) [22] and the Velocity Filter Analyser (VFA) [23], were used to collect the experimental fast neutral data. The analysers scanned horizontally along the torus equatorial plane, the MEA from R_t = 8 cm to R_t = 42 cm and the VFA from R_t = 49 cm to R_t = 93 cm, where R_t is the tangency major radius of the viewing chord. The data acquisition system allowed for fast data collection up to 10 kHz. With the exception of the neutron measurements during beam turnoff experiments, all the data presented here were averaged over several milliseconds. A vertically viewing diagnostic neutral beam (DNB) at R = 96 cm was used in some of the discharges to localize the measurements to the plasma centre. The DNB enhanced the H^0 flux from the main beams by adding a source of D^0 neutrals in a small region ($r \approx 6$ cm) close to the magnetic axis. Subtracting the H^0 flux measured with the DNB off from that measured with the DNB on (at the same energy setting) yields the flux originating from charge exchange events between beam ions in the plasma core and DNB neutrals reaching the torus equatorial plane.

2.2. Methods

To determine whether the fast ion behaviour is classical, the fast neutral spectra are compared with the predictions of the orbit following Monte Carlo code NEWORBX. This code is based on the original version written by Goldston et al. [24], and it was subsequently modified by Fowler and Rome [25] to account for non-circular, non-concentric magnetic surface geometry.

NEWORBX uses the magnetic surface geometry obtained through a solution of the Grad-Shafranov equation that is consistent with experimental measurements. Russian roulette and particle splitting schemes [17] were implemented in the calculation of the fast ion distribution function to improve the statistical quality of the Monte Carlo estimates and thereby to obtain smooth simulated spectra of perpendicularly scattered ions. The electron density and temperature profiles $[n_e(r), T_e(r)]$ were determined experimentally by the Thomson scattering diagnostics. The background neutral density profile $n_0(r)$ was calculated by the one-dimensional cylindrical code NEUCG [26]. Previous calculations of $n_0(r)$ performed with a two-dimensional Monte Carlo code [22] showed that the one-dimensional results were quite adequate for the analysis of charge exchange spectra if the central neutral density was left as a free parameter. In fact, although the two-dimensional calculation predicted large toroidal asymmetries in the magnitude of the background neutral density, depending on the distance from the gas sources, it also showed that the neutral density *profiles* were independent of the distance from the sources. A three-dimensional analysis for $n_0(r)$ was deemed unnecessary in view of the fact that the NPAs were at some distance from the limiters and the gas valve (approximately 140° and 60°, respectively) and that the fast neutral spectra obtained with the NEUCG calculation of $n_0(r)$ were in good agreement — in the shape and separation of the spectra along different viewing chords — with the experimental results. A beam halo contribution was included in the calculation of $n_0(r)$ for the charge exchange losses, but only the wall source was used to calculate the fast neutral flux to the NPA, Φ_0, since the analysers were located several neutral mean free paths away from the injection points of the beam lines. The magnitude of the wall source was obtained by multiplying the measured gas puff rate Φ_g by a coefficient necessary to match the experimental Φ_0 in absolute magnitude. Physically, this coefficient is related to the wall recycling coefficient R and to the toroidal distance from the gas valve. The multipliers used for the estimation of the charge exchange losses and the flux to the NPA were chosen independently because the former reflects a volume averaged quantity while the latter is localized toroidally. Values between 0.4 and 2.5 times Φ_g were used, with variations qualitatively consistent with changes in recycling inferred from the $\Phi_g(t)$ trace and the $H_\alpha(t)$ signals at various toroidal locations. For H^+ ions striking a stainless steel wall with energies in the range from 10 eV to 100 eV, the reflection coefficient (most of the particles are reflected as neutrals) goes roughly from 0.5 to 0.8 [27, 28]. These values correspond to Φ_g multipliers between 2 and 5. However, the recycling takes place mostly in the limiter region, whereas the neutral source away from the limiter (and the gas valve) is significantly smaller. The edge neutral energy was taken to be 10 eV, consistent with previous experimental measurements [29].

As a further tool to verify the validity of classical theory, the predicted and experimentally observed beam–plasma neutron emissions during injection of beams doped with 3% D^0 were compared. Measurements of the decay rates in the beam–plasma neutron emission following turnoff of the doped beam yielded information on the slowing-down process.

3. EXPERIMENTAL RESULTS

3.1. I_p scan for co-injection

For the investigation of fast ion confinement, low-I_p discharges are of interest because orbit displacements from the magnetic surfaces are maximized and larger orbit losses are expected. For a typical, low-I_p case (I_p = 100 kA), an estimate of the orbit displacement yields $\epsilon\rho_p/a \simeq 0.8$ for a 30 keV passing proton close to the plasma edge (ϵ is the inverse aspect ratio, ρ_p is the poloidal gyroradius, and a is the plasma minor radius) and correspondingly larger orbit widths for trapped particles. More generally, the discharge characteristics varied strongly with I_p in ISX-B, and it is important to probe whether classical theory describes the fast ion behaviour equally well in both low- and high-I_p cases. Low-I_p discharges, typically, had lower τ_E^*, higher β_p, lower $T_e(0)$ and $T_i(0)$, and more peaked profiles than high-I_p discharges. The MHD activity was also typically different [30]. Two sets of experiments were performed on the ISX-B to investigate beam ion confinement at low and relatively high I_p, one with co-injection and the other with counter-injection. Fast neutral spectra were obtained in low- and relative high-I_p discharges and were matched with the corresponding predictions of the NEWORBX code. The co-injection case is considered first, while the counter-injection case is discussed in Section 3.2. An effort was made to keep the external plasma parameters (B_t, $\bar{n}_e$, etc.) as close as possible between the high- and low-I_p sequences. The time histories of some of the discharge characteristics for the co-injection experiment are displayed in Fig. 2. The Thomson scattering profiles were taken at 190 ms and are shown in Fig. 3. The experimental

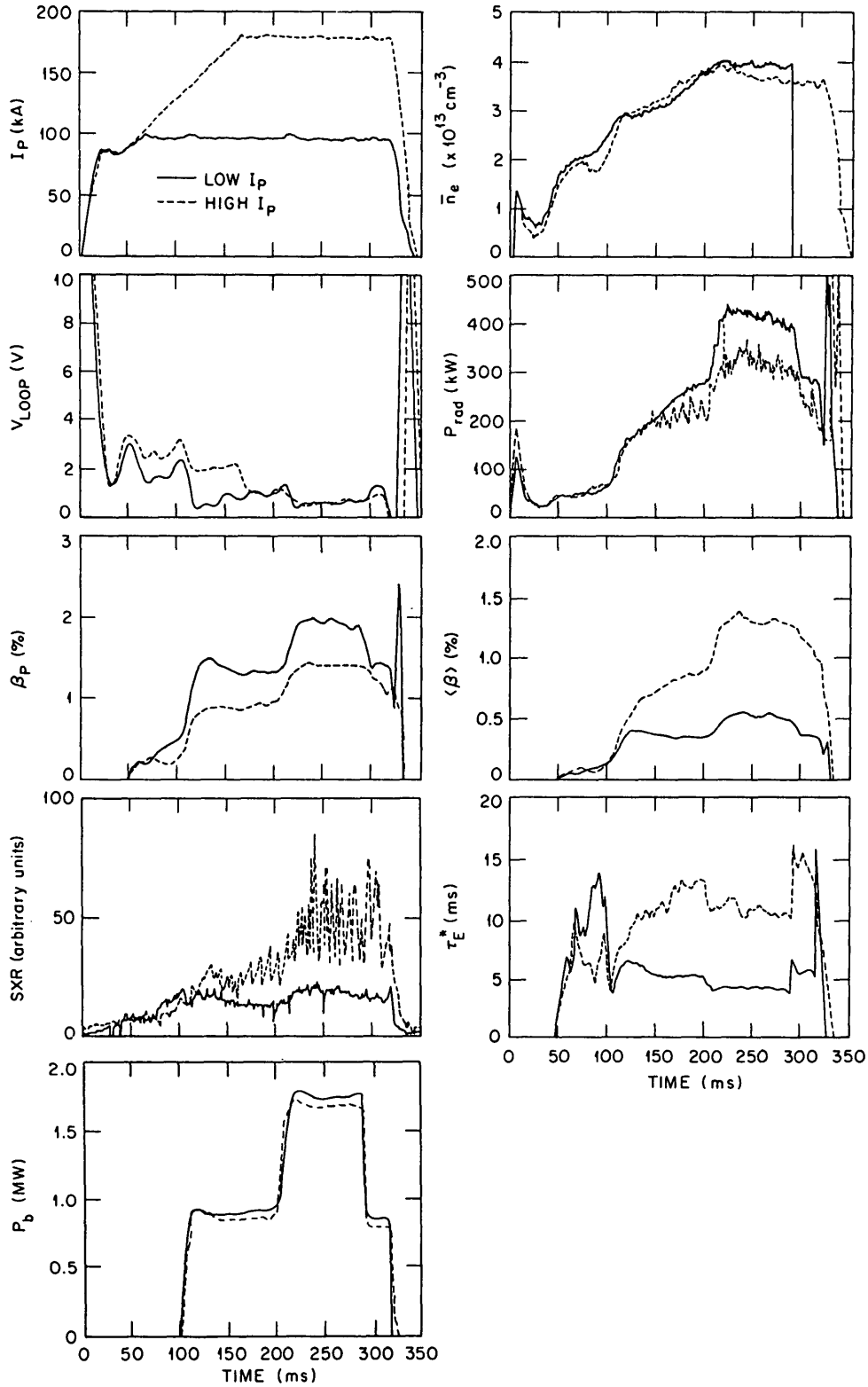

FIG. 2. Time histories of plasma parameters for the low- and high-I_p comparison during co-injection. Thomson scattering profiles were taken at 190 ms. B_t = 1.38 T for both sequences. Thomson scattering profiles were also taken at 280 ms, for the beam additivity experiment. (The sudden termination of the $\bar{n}_e$ trace for the low-I_p case at $t \simeq$ 290 ms is due to software processing.)

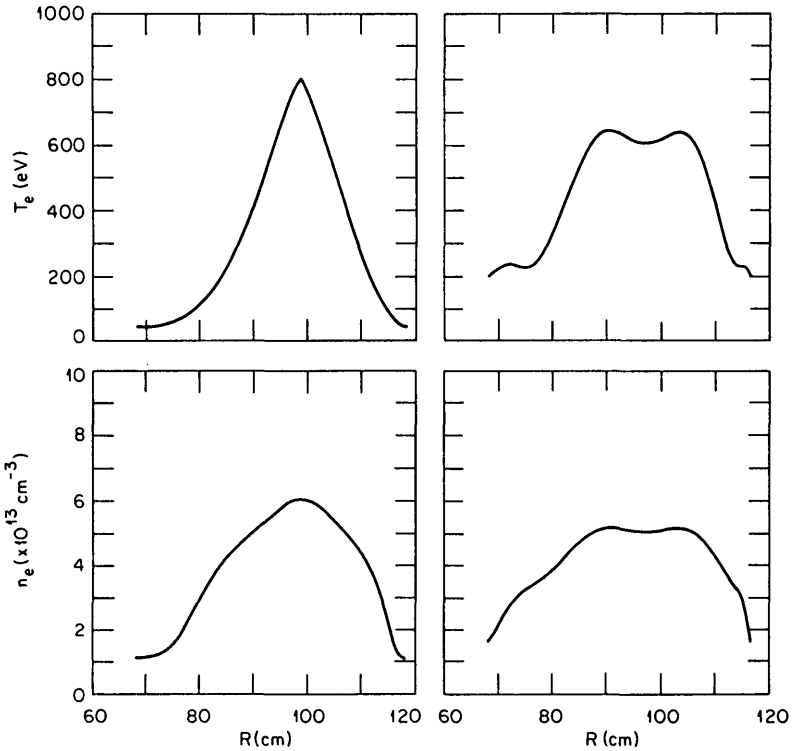

FIG. 3. Fitted profiles to the Thomson scattering data for the one-beam phase of the I_p = 96 kA (left) and I_p = 180 kA (right) co-injected discharges.

fast neutral spectra measured along three viewing sightlines for the two cases (at 190 ms) are shown in Fig. 4, superimposed on one another to display the changes that occurred when I_p was varied. The VFA was limited to a maximum energy of ~27 keV, because of damage having occurred in one of its channeltron detectors.

The spectra for the high-I_p case are compared with the corresponding Monte Carlo simulation in Fig. 5(a). A Φ_g multiplier of 1.67 — corresponding to a recycling coefficient R = 0.4 — was used to calculate $n_0(r)$ for both the charge exchange losses and Φ_0. Z_{eff} = 1.02 was inferred from plasma resistivity and includes a correction for electron trapping. In general, the fast neutral spectra were not strongly sensitive to Z_{eff} [17], because, owing to the relatively low average values of T_e and, therefore, of $E_{critical}$, the slowing-down process was dominated by collisions with electrons. The simulation is in excellent agreement with the experimental data in the shapes and separation of the spectra, with the absolute magnitude of the flux fixed by a reasonable choice for the Φ_g multiplier, as was discussed in Section 2.2. The agreement is particularly significant because ions scattered over a wide range in pitch angle contribute to these spectra. The R_t = 72 cm sightline samples ions that are almost undeflected from their original directions ($v_\parallel/v$ ~ 0.65), whereas the flux along the R_t =8.5 cm chord originates from ions that have scattered considerably in pitch angle ($v_\parallel/v$ ~0.1).

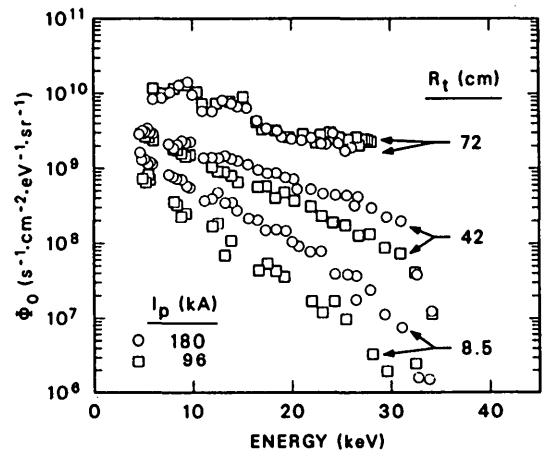

FIG. 4. Experimental fast neutral spectra obtained during co-injection at high and low I_p. The other external plasma parameters were the same for the two sequences. The tangency radii of the viewing chords are — from top to bottom — R_t = 72, 42 and 8.5 cm. At low I_p, enhanced orbit losses of ions with $v_\parallel/v \ll 1$ are evidenced by the flux depletion along the perpendicular and quasi-perpendicular sightlines.

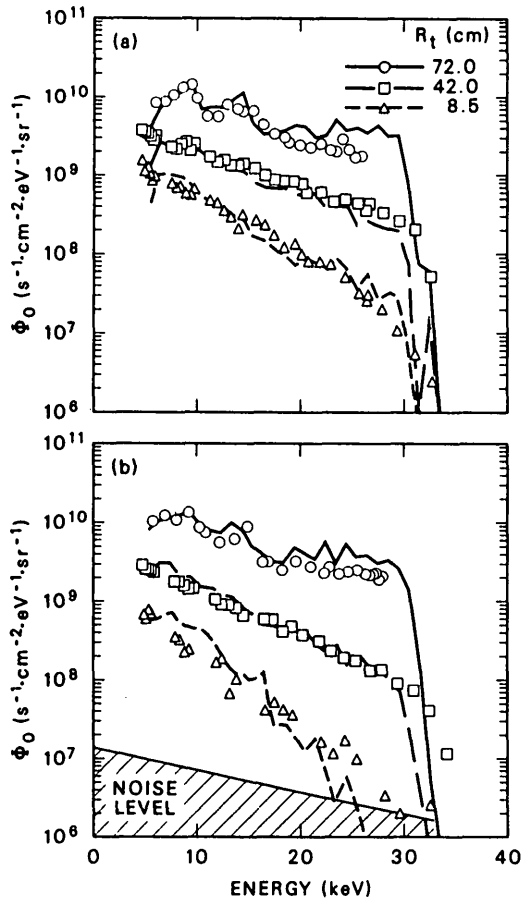

FIG. 5. Comparison of experimental and predicted fast neutral spectra during co-injection at high and low I_p. (a) I_p = 180 kA; (b) I_p = 96 kA. The tangential NPA (R_t = 72 cm) was limited to a maximum energy of ~27 keV.

The width of the high energy tail above E_{inj} (30.2 keV) along the R_t = 42 cm chord appears to be larger than predicted. This was observed generally in all experiments and for all sightlines and is partly attributable to the energy resolution of the NPA ($\Delta E/E \geq 5\%$). Furthermore, there are indications that this energy region is undersampled in the Monte Carlo calculation, because of poor counting statistics (an energy diffusion term is included in the Monte Carlo code). Simulations limited to the high energy portion of the spectra, but obtained by using a larger number of launched particles, produced somewhat wider tails. The remaining discrepancy at energies above E_{inj} may be due to the neglect of collisions between the beam particles themselves in the NEWORBX code.

The corresponding comparison between measured and calculated charge exchange spectra for the low-I_p case is shown in Fig. 5(b). Here, the Φ_g multiplier was also set to equal 1.67 for both $n_0(r)$ profiles. Z_{eff} was estimated to be 1.1. The Monte Carlo simulation correctly predicts that the tangential spectrum is unaffected by the change in I_p. The fast neutral signal along the tangential sightline is produced mostly by co-passing ions that charge exchange promptly near the outer edge of the torus, as shown in Fig. 6, which displays the fast neutral flux origination profiles obtained from the Monte Carlo simulation for the low-I_p case. The high background neutral density near the plasma edge and the fact that the ions attain there the proper pitch angle to be detected along the tangential chord determine the spectrum, which is therefore relatively insensitive to changes in the boundaries of the

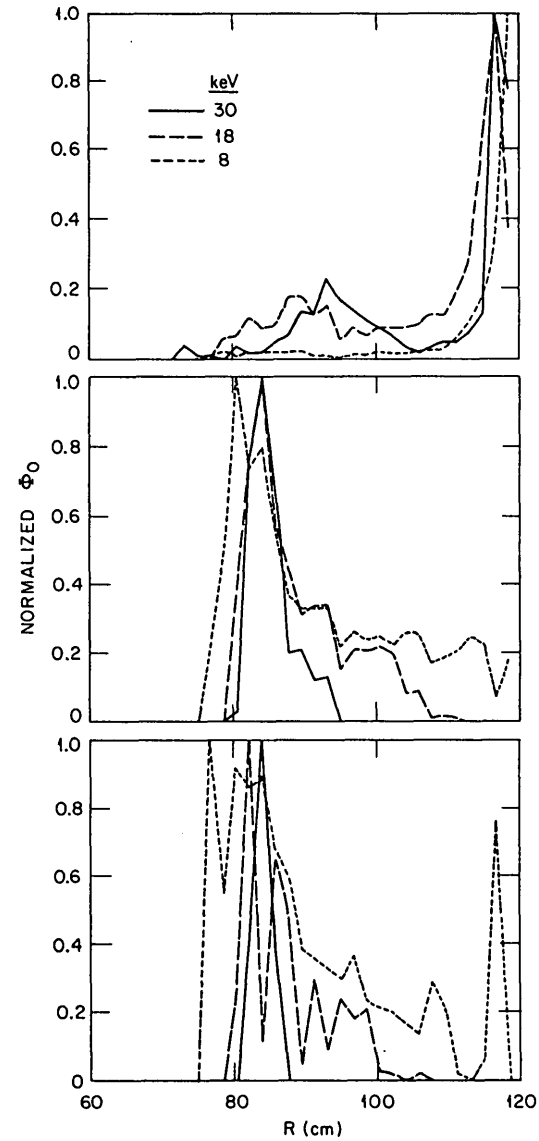

FIG. 6. Neutral flux origination profiles during co-injection at low I_p (96 kA). Top: R_t = 72 cm; centre: R_t = 42 cm; bottom: R_t = 8.5 cm.

loss region near the inner edge of the torus resulting from different values of I_p. The portion of tangential fast neutral flux that originates from a broad band near the plasma centre comes from co-passing ions circulating on small, well confined orbits. These orbits are far from the loss region and remain essentially unaffected by the lower I_p. Experimentally, the increased orbit losses at low I_p are reflected in a lower fast neutral flux along the more perpendicular viewing chords, especially in the high energy portion of the spectra. This is well reproduced by the Monte Carlo simulation. The fact that the experimental flux at high energy and along the most perpendicular sightline is higher than predicted is partly a consequence of the low signal-to-noise ratio. Also, the statistical uncertainty is significant for both the experimental data and the Monte Carlo simulation in that region.

A comparison of the power delivered to the plasma and power losses for the two I_p values — as calculated by the NEWORBX code — is presented in Table I. Total orbit losses amount to less than 10% of the injected power, even for the low-I_p case. However, the high energy perpendicular NPA signal is affected strongly by the increased prompt losses because these directly affect the fast ion population that contributes the largest portion of that signal. (In NEWORBX, prompt orbit losses are defined as those with ions that exit the plasma before the fifth crossing of the equatorial plane.) In fact, the high energy perpendicular flux originates from ions born at the outer edge of the plasma that charge exchange promptly on the inside legs of their orbits — with pitch angles readily detectable by the perpendicular NPA — close to the boundary of the loss region. This is shown in Fig. 6, interpreted with the help of Fig. 7 (after Rome et al. [31]), which depicts the orbit topology for a 10 keV proton in a plasma equilibrium that represents, in a qualitative fashion, much of the ISX-B data. In Fig. 7, the co-injected beam would be represented by a line close to the R_t = 72.5 cm line. 10 keV ions born at R ~ 120 cm (with $v_\parallel/v \simeq 0.62$) follow orbits that cross the torus midplane on the inside at R ~ 80 cm with $v_\parallel/v \sim 0.3$, and thus require little scatter in phase space to be detected along the R_t = 8.5 cm chord. At higher energies, the loss region widens and the fast ions reach the perpendicular viewing sightlines at increasingly larger major radii. This is illustrated by the flux origination profiles in Fig. 6. At lower I_p, the loss regions for any given energy become wider. Also, because of the larger orbits shifts, the inner crossing of the torus midplane occurs at a larger major radius and correspondingly larger initial pitch angle there, so that considerable pitch angle scattering is required before the ions reach the perpendicular sightline. Thus, as lower plasma currents and higher ion energies are considered, the ions that contribute the most to the perpendicular fast neutral flux suffer increasingly

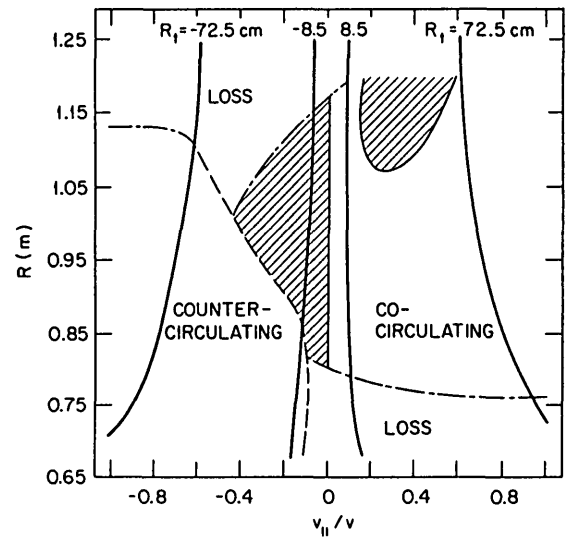

FIG. 7. Four representative NPA sightlines superimposed on the orbit topology for a 10 keV proton (after Rome et al. [31]). Shaded areas represent the trapped particle regions. A low β (0.3% volume averaged), low current (I_p = 110 kA) equilibrium was used for the calculation.

TABLE I. POWER DISTRIBUTION (IN PER CENT OF INJECTED POWER) FOR CO-INJECTED HIGH- AND LOW-I_p DISCHARGES

	I_p = 180 kA	I_p = 96 kA
P_{be}	57.6	60.9
P_{bi}	28.3	21.2
P_{cx}	4.4	4.1
Shinethrough	2.0	3.3
Total orbit losses	3.5	8.1
Prompt orbit losses	2.8	7.9
Non-prompt orbit losses	0.7	0.2
P_{OH}	0	-0.1
P_{therm}	4.2	2.5

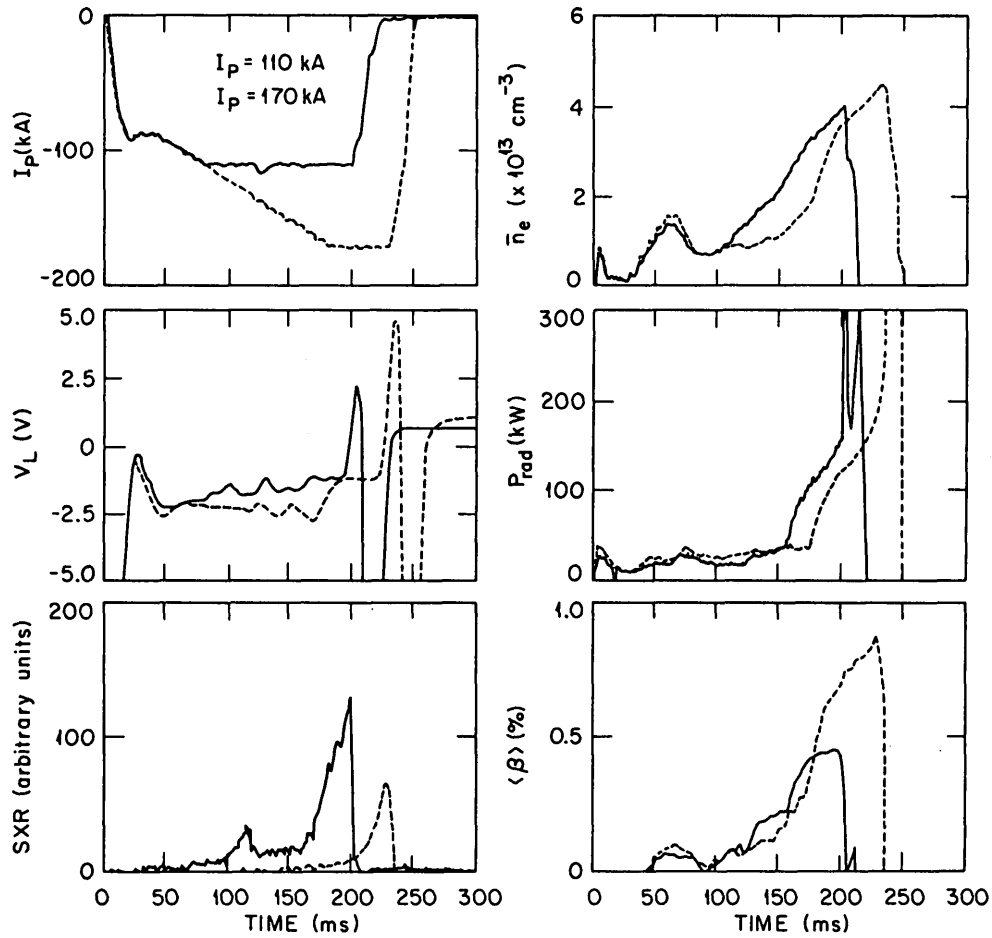

FIG. 8. Time histories of plasma parameters for the low- and high-I_p comparison during counter-injection. Thomson scattering profiles were taken at 190 and 215 ms, respectively.

larger losses, and the resulting flux is reduced. Equally important is the fact that — at low I_p — the peak contribution to the near-perpendicular fast neutral flux comes from regions of larger major radius, and correspondingly smaller minor radius, due to the changing boundary of the loss region. (This can be seen, for example, by comparing Figs 6 and 16.) The product of background neutral density and attenuation integral ($n_0(r)\exp(-\int n\sigma ds)$), which is proportional to the detected flux, is estimated to be approximately 2.5 times lower at R = 85 cm than it is at R = 80 cm for a 30 keV proton along the R_t = 8.5 cm sightline in these plasmas [17], resulting in a comparable reduction in the perpendicular fast neutral flux in the I_p = 96 kA discharge as compared to the I_p = 180 kA case, even without including the decrease in the fast ion density due to scattering into the loss region. In summary, we find that fast ion behaviour is well explained classically even in the low-I_p, large orbit width regime.

The fraction of the total power deposited in the plasma at low I_p is only slightly lower than in the high-I_p case — 82% as opposed to 86%. A somewhat larger fraction of the deposited power goes to the electrons at low I_p — 74% versus 67%. This is a consequence of the lower T_e and correspondingly lower $E_{critical}$. The volume averaged electron temperatures from Thomson scattering measurements were 258 eV and 364 eV for I_p = 96 kA and 180 kA, respectively. The larger amount of power that thermalizes (i.e. beam ions that reach the bulk ion temperature) in the I_p = 180 kA sequence is an indicator of the better confinement properties of higher I_p discharges.

3.2. I_p scan for counter-injection

Purely counter-injected discharges in the ISX-B always disrupted within ≤50 ms from the beginning of injection. They were characterized by high levels of

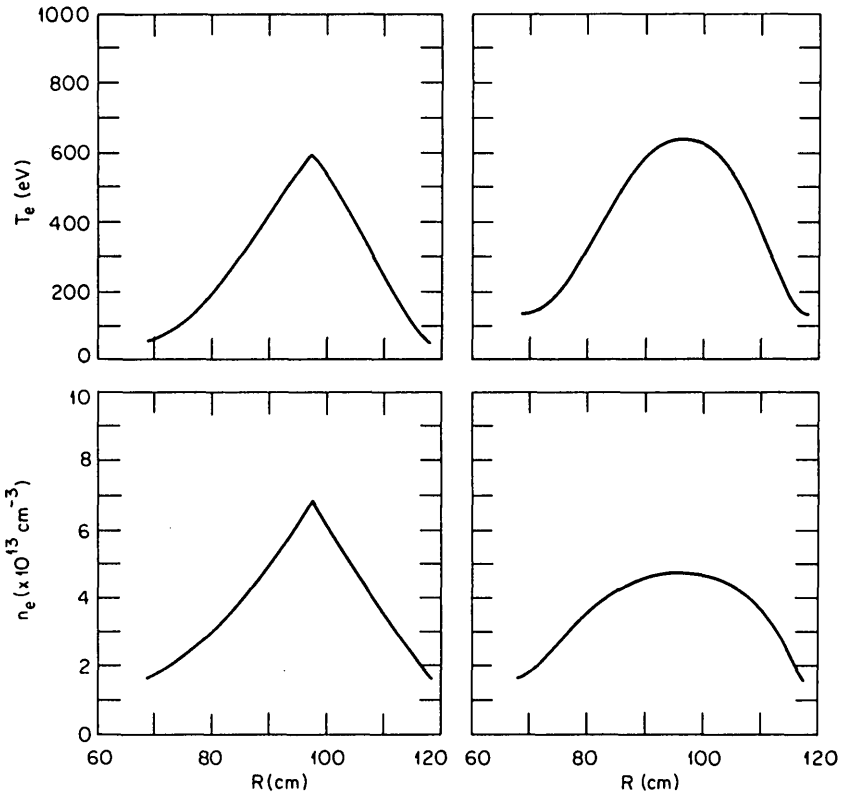

FIG. 9. Fitted profiles to the Thomson scattering data for the I_p = 110 kA (left) and I_p = 170 kA (right) counter-injected discharges.

impurity accumulation in the plasma core [32], high radiated powers, and low electron and ion temperatures. These discharges were typically run at low beam power, medium densities, and medium to high plasma currents. Gettering was also required.

Counter-injection in low-I_p discharges provides a suitable scenario for testing the theory of the beam thermalization process under the most severe conditions of fast ion confinement, because of the increased importance of the orbit loss regions [17, 33]. Two experiments were specifically dedicated to the investigation of beam ion confinement during counter-injection, one at I_p = 170 kA, the other at I_p = 110 kA. These experiments were performed consecutively on the same day. Discharge characteristics for the two sequences are displayed in Fig. 8. The laser times for the Thomson scattering profiles, shown in Fig. 9, were 215 ms for the high-I_p case and 190 ms for the low-I_p case. B_t ($\simeq$12.3 kG), $\bar{n}_e$ ($\simeq 3.8 \times 10^{13}$ cm^{-3}), P_b ($\simeq$0.5 MW), and E_{inj} ($\simeq$28.8 keV) were approximately the same for both sequences at corresponding laser times. The comparison of the Monte Carlo simulation with the experimental spectra is shown in Fig. 10(a) for the high-I_p case and in Fig. 10(b) for the low-I_p case. The VFA flux (R_t = −72 cm) was lowered by 40% compared to the raw data in both comparisons. This correction is within the error bars, considering that (1) an a posteriori analysis showed that the VFA gas flow rate in the NPA neutralization cell was monitored with an uncertainty of ±40% and (2) the wall neutral source may be somewhat different at the MEA and VFA locations. The background neutral density profiles used to calculate the charge exchange losses were determined by assuming a Φ_g multiplier of 2.5. This value may be somewhat too high, considering that a Φ_g multiplier less than unity was used for calculating Φ_0. However, charge exchange losses constitute only a small fraction of the power balance in these discharges and, furthermore, the calculated spectra were not very sensitive to charge exchange losses. To match Φ_0 in magnitude, the Φ_g multiplier was assumed to be 0.55 for the I_p = 170 kA case and 0.4 for the I_p = 110 kA case. The values of Z_{eff} inferred from plasma resistivity were 1.9 for the high-I_p case and 1.5 for the low-I_p case. Good agreement is observed between the predicted and the experimental spectra at both I_p

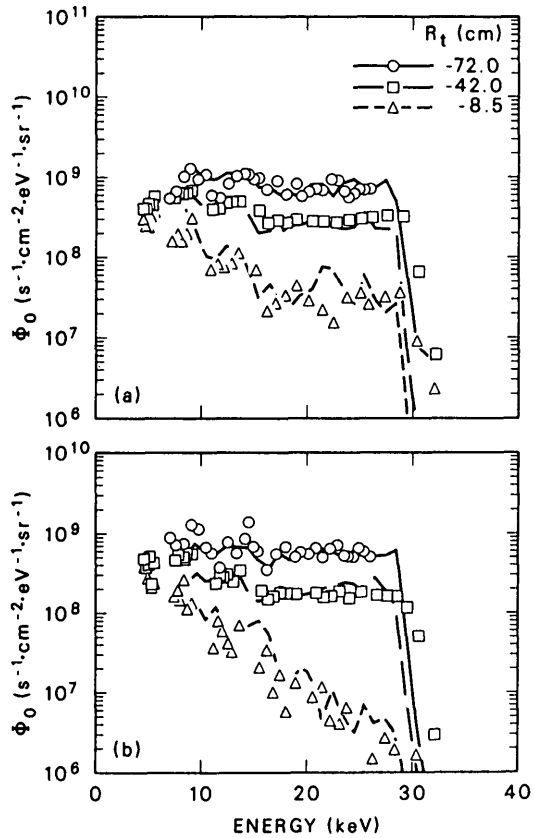

FIG. 10. Comparison of experimental and predicted fast neutral spectra during counter-injection at high and low I_p. (a) I_p = 170 kA; (b) I_p = 110 kA. Injection was at R_t = −74.5 cm.

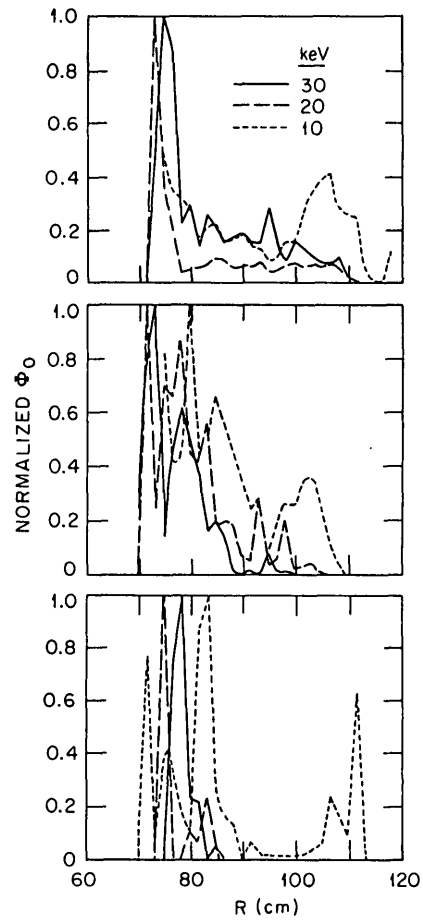

FIG. 11. Neutral flux origination profiles during counter-injection. Top: R_t = −72 cm; centre: R_t = -42 cm; bottom: R_t = − 8.5 cm. Plasma parameters were $\bar{n}_e = 3.8 \times 10^{13}$ cm^{-3}, I_p = 110 kA, B_t = 1.23 T. The plasma edge is at R ≃ 68 cm.

settings. Comparing the experimental spectra obtained during co-injection with those obtained during counter-injection, the latter are seen to have a flatter appearance. This difference is reproduced closely by the Monte Carlo simulation and is, therefore, attributable to classical processes. The larger orbit losses — in particular, the prompt loss of fast ions born near the peripheral region on the outside of the torus — and the shorter slowing-down times in counter-injection discharges reduce the fast-ion population at energies away from E_{inj}, thus lowering the resulting fast neutral flux.
It may also be noted that the code properly predicts the large decrease in the high-energy perpendicular flux along the R_t = −8.5 cm chord during counter-injection at low I_p with respect to the high-I_p case. The depletion is caused by the loss region boundary (on the inside of the magnetic axis) crossing the perpendicular sightline at the lower I_p setting [17], as can be inferred from Fig. 7, considering that the boundary of the loss region near R ~ 70–80 cm and $v_\parallel/v \sim -0.1$ will move to larger negative values of $v_\parallel/v$ as I_p is lowered. One interesting result of the Monte Carlo simulation is that, during tangential counter-injection, the largest part of the fast neutral flux for *all* sightlines with −72 cm < R_t < −8 cm comes from a region close to the plasma edge on the inside of the torus, as shown in Fig. 11; this is a consequence of the presence of a loss region near the outer edge of the torus for counter-injection and the steep increase of $n_0(r)$ with minor radius. The calculated powers for the high- and low-$I_p$counter-injected cases are summarized in Table II. Orbit losses account for a considerable portion of the injected power during counter-injection, especially at the lower I_p setting — 34% of the total power. Even in the regime of poorest orbit confinement, classical theory provides a good account of fast ion behaviour.

TABLE II. POWER DISTRIBUTION (IN PER CENT OF INJECTED POWER) FOR COUNTER-INJECTED HIGH- AND LOW-I_p DISCHARGES

	I_p = 170 kA	I_p = 110 kA
P_{be}	43.5	42.2
P_{bi}	19.0	14.3
P_{cx}	6.6	4.8
Shinethrough	3.3	2.8
Total orbit losses	24.4	33.9
Prompt orbit losses	17.4	23.8
Non-prompt orbit losses	7.0	10.1
P_{OH}	1.5	1.0
P_{therm}	1.7	1.0

3.3. Beam-plasma neutron emission measurements

A well established method for investigating the confinement of the beam ions, in addition to the analysis of fast neutral spectra, is the measurement of beam-plasma neutron emission [11, 12, 34, 35]. Typically, the experimental measurements are compared with computations based on classical beam capture and slowing-down, thus testing whether classical processes govern the behaviour of the energetic particles. The comparison is sensitive to the deposition profile of the full energy component of the beam and to the first stages of the slowing-down of full energy ions circulating in the plasma core. Two sets of experiments are presented here. First, absolute measurements of the beam-plasma neutron emission are considered. A comparison is presented between the set of all the ISX-B data and the corresponding predictions of the Monte Carlo code. The limitation of comparing absolute neutron emission levels to infer possible fast ion losses is that the uncertainty for both the measured and calculated neutron emission is quite large; we estimate an uncertainty of $\sim \pm 40\%$ in the calculation (due to uncertainties in n_H/n_D, beam fractional energy composition and D^0/H^0 fraction, calculated beam deposition profiles, and experimental measurements of $T_e(r)$ and $n_e(r)$) and $\pm 25\%$ in the measurement [17]. Then, experiments aimed at verifying that the beam ions slow down according to classical theory are discussed. The decay time in the beam-plasma neutron emission following a sharp beam turnoff — as predicted by the time dependent Fokker-Planck code FPP (originally developed by R. Goldston at Princeton) — is compared with the experimentally measured value for several different discharges. The experimental uncertainty is $\sim 30\%$, while the calculated values rest on the assumption that the plasma profiles do not change appreciably during one neutron emission decay time τ_N ($\tau_N \sim \tau_{se}/14$ on ISX-B, where τ_{se} is the slowing-down time on electrons).

The experimental measurements of the neutron emission collected under a variety of plasma and beam parameters and injection geometries are matched with the values predicted by NEWORBX in Fig. 12. The thermonuclear yield — measured at the laser time during injection of 100% H^0 beams in similar discharges — has been subtracted from the experimental data (and it has not been included in the Monte Carlo calculation) so that each point in the plot represents the beam-plasma neutron intensity for a particular plasma sequence. Circles refer to data taken during co-injected discharges, and squares refer to discharges with balanced injection. The beam-target relative velocity was corrected for toroidal plasma rotation in the co-injection discharges. The target dilution due to beam hydrogen and hydrogen desorption from the walls was assumed to be $\sim 30\%$ (i.e. $n_D/(n_D + n_H) \sim 0.7$). In all cases when two beams were injected, only one beam was doped with 3% D^0, the other being 100% H^0. Because of the small ratio of fast ion density to target density, beam-beam reactions have been neglected.

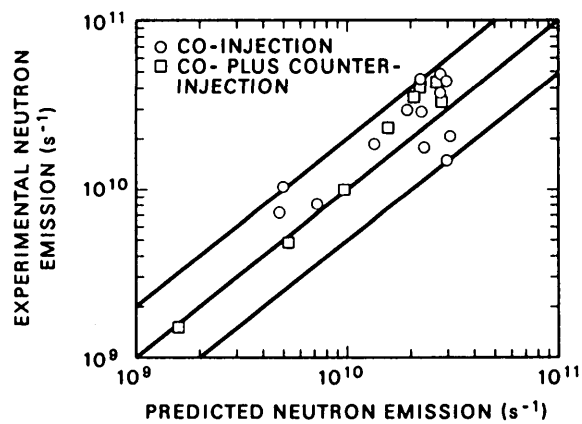

FIG. 12. Comparison of experimental and predicted beam-plasma neutron emission. The central solid line corresponds to one-to-one agreement, while the other two lines represent a discrepancy by a factor of 2.

TABLE III. RANGE OF PARAMETERS FOR THE COMPARISON IN Fig. 7

Line averaged electron density	$1.4 \times 10^{13} < \bar{n}_e < 7 \times 10^{13}$ cm^{-3}
Plasma current	$96 < I_p < 190$ kA
Toroidal magnetic field	$1.2 < B_t < 1.4$ T
Central electron temperature	$630 < T_e(0) < 950$ eV
Central ion temperature	$530 < T_i < 1330$ eV
Injected beam power	$0.46 < P_b < 1.8$ MW
Beam energy	$18.4 < E_{inj} < 31.2$ keV

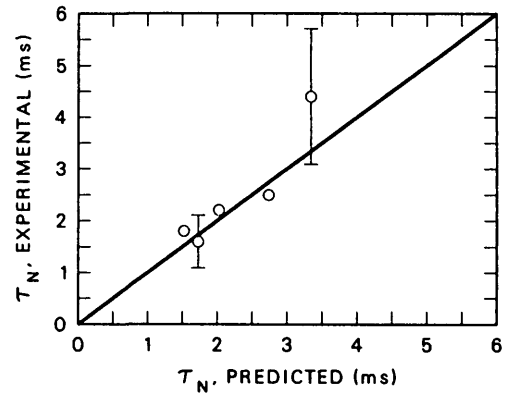

FIG. 13. Comparison of experimental and predicted decay times (τ_N) of the beam-plasma neutron emission for five different plasma discharges. The Thomson scattering radial profiles of T_e and n_e were used in the calculation.

For all points in the plot except one, the doped beam was co-injected. The range in plasma and beam parameters encompassed by this comparison is displayed in Table III.

Theory and experiment agree within a factor of ≤ 2. The large number of variables that enter the theoretical calculation and the uncertainties associated with them may account for a discrepancy of that magnitude. Therefore, within the error bars, the Fokker-Planck theory accounts for the confinement and initial slowing-down of the beam ions in the plasma core. The amount of data available was too limited to detect any significant dependence of the relative agreement between theory and experiment on P_b, I_p, $\bar{n}_e$, or the injection geometry.

In some of the experiments, the beam doped with deuterium was turned off immediately after the time at which the Thomson scattering profiles were taken, and the decay of the neutron emission was monitored. The profiles were then used in the Fokker-Planck code to calculate the predicted decay rates. The discharges lasted, typically, ≥ 10 ms after the beam turnoff. The thermonuclear neutron yield was assumed to remain constant during the decay time τ_N. This is not a bad assumption, considering that the energy confinement time was ~ 10–15 ms, whereas $\tau_N \lesssim 3$ ms, and, therefore, no significant cooling is expected during $1\tau_N$. (In one case the thermonuclear emission was monitored after turnoff of one of two 100% H^0 beams, and it was seen to remain constant for $\sim 1\tau_N$, decreasing by only $\sim 20\%$ in a time $2\tau_N$.) Figure 13 shows the resulting experimental and predicted values of τ_N. The good agreement between the Fokker-Planck prediction and the data indicates that classical theory describes well the initial slowing-down of the beam ions.

3.4. Beam additivity

This section deals with whether the beam ion confinement was independent of the injected beam power in the ISX-B. Two sets of discharges were executed, one at $I_p = 96$ kA and the other at $I_p = 180$ kA. The time histories of the plasma parameters for the beam additivity experiments are those shown in Fig. 2. B_t was constant at 13.8 kG. Thomson scattering profiles for the two-beam phase of the discharges are shown in Fig. 14. Only the results obtained in the high-I_p sequence are presented here. The experiment at low I_p produced results similar to those at high I_p. The west beam was co-injected at 100–286 ms (H^0, 30 keV, 850 kW), and the east beam was co-injected at 200–316 ms (H^0, 30 keV, 800 kW). The line averaged electron density (3.8×10^{13} cm^{-3}) and the plasma current were kept approximately constant from 180 ms on. The DNB (D^0, $E_{inj} \sim 25$ keV) was used in some of the shots to localize the fast H^0 flux measurements to the plasma centre. Line integrated as well as localized spectra were compared at 190 and 280 ms, during injection of one and two beams, respectively. Thomson scattering profiles were taken at these time points. To gather further information from these experiments, the west beam was doped with 3% D^0.

The experimental, line integrated, fast neutral flux went up by factors of ≥ 2 along all viewing chords as the second beam was added to the first. An enhancement by factors other than 2 is possible because of changes induced by the second beam in the $T_e(r)$, $n_e(r)$ and $n_0(r)$ profiles. Injecting two beams of equal power —

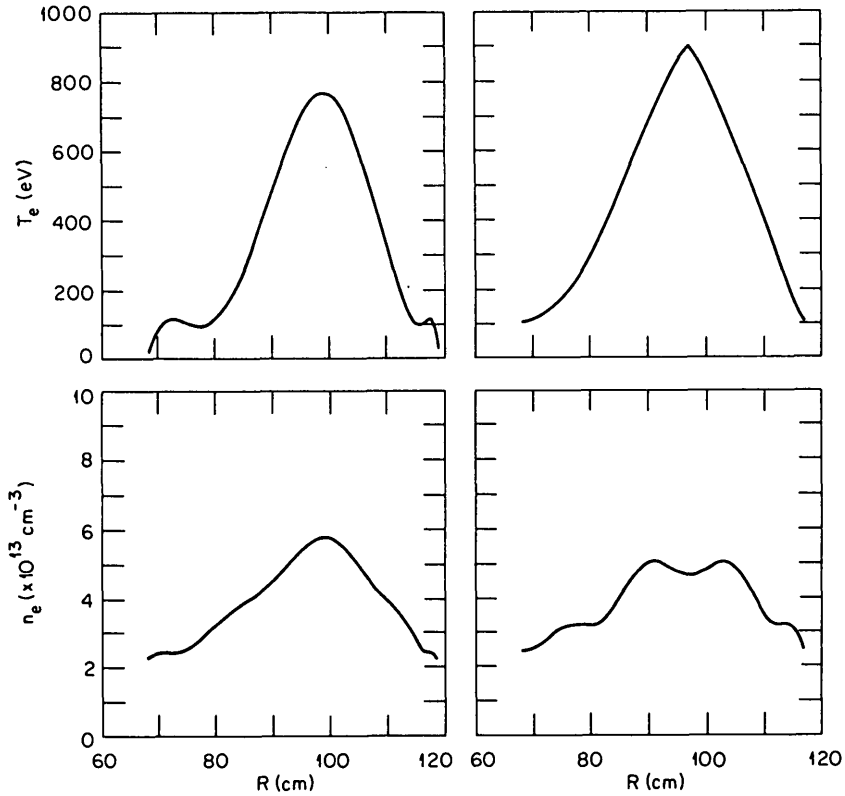

FIG. 14. Fitted profiles to the Thomson scattering data for the two-beam phase of the I_p = 96 kA (left) and I_p = 180 kA (right) co-injected discharges.

while holding the external plasma parameters constant — produced line integrated, fast neutral fluxes at least twice as large as those observed when only one beam was injected. This suggests that the fast ion density is proportional to the injected beam power, if changes in $T_e(r)$ and $n_e(r)$ are taken into account. To prove that this is in fact the case, the experimental spectra were compared with the predictions of the Monte Carlo estimation, which used the $T_e(r)$ and $n_e(r)$ profiles determined experimentally at 190 and 280 ms. A wall recycling coefficient of 0.4 was assumed in the calculation of $n_0(r)$ for the charge exchange losses as well as for the flux to the NPA at both time points. (Only a small increase in recycling in the two-beam phase was inferred from the $\Phi_g(t)$ and $H_\alpha(t)$ traces.) As shown in Fig. 15, the NEWORBX simulation is in good agreement with the experiment during both one- and two-beam phases, providing strong evidence that, globally, the fast ion confinement did not deteriorate with increasing P_b. It should, however, be noted that the fast neutral flux origination profiles, displayed in Fig. 16, show that most of the flux originated from regions away from the plasma centre for all viewing chords, and thus is not directly representative of the fast ion behaviour in the plasma core.

In contrast to the passive, line integrated data, the localized flux measurements were contrary to expectations. A perpendicular spectrum was obtained using the DNB to localize the measurement to the plasma centre (a tangential spectrum with the DNB on was also obtained, but it could not be used because the channeltron detectors reached counting saturation during the two-beam phase). The MEA sightline intercepts the DNB centreline at $R_t \simeq 8.5$ cm. As displayed in Fig. 17, the perpendicular neutral flux originating from the plasma centre showed little increase with the second heating beam, unlike the line integrated flux. When compared with the predictions of the Monte Carlo calculation, the localized spectrum was reproduced with a lower degree of accuracy than the passive spectra. However, the simulation indicated that the localized flux, during two-beam injection, should be a factor of ~ 3 higher than during one-beam injection, contrary to the experimental evidence. Therefore,

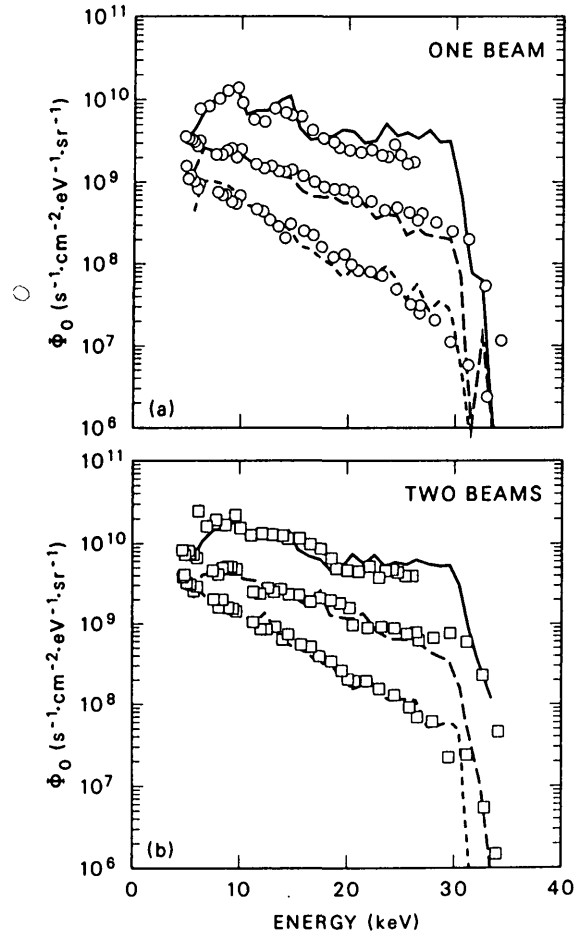

FIG. 15. Comparison of experimental spectra with the predictions of the Monte Carlo calculation during (a) one-beam and (b) two-beam injection. Line integrated spectra at R_t = 72, 42 and 8.5 cm.

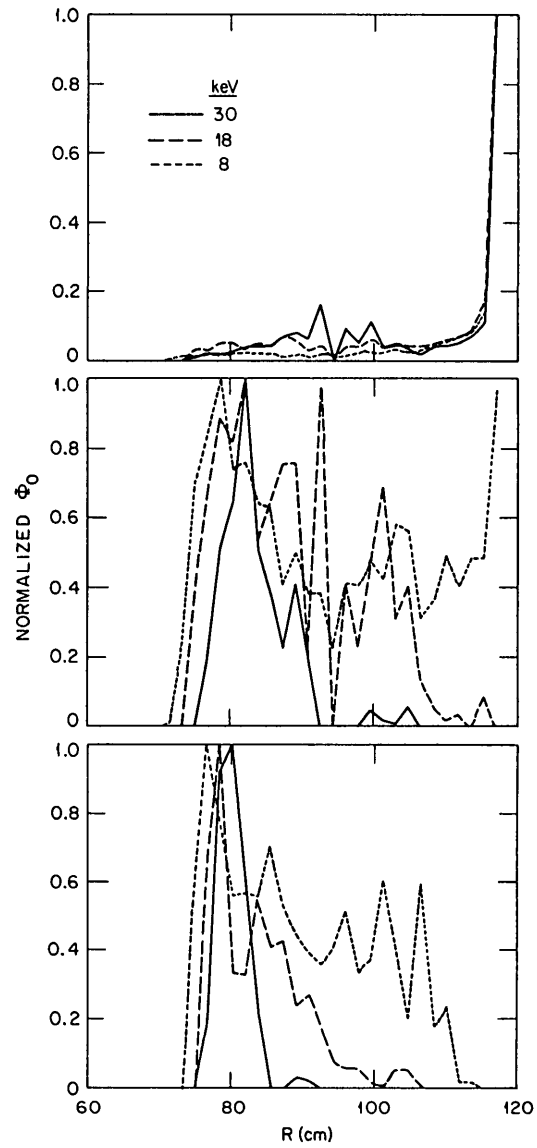

FIG. 16. Neutral flux origination profiles during two-beam co-injection at relatively high I_p (180 kA). Top: R_t = 72 cm; centre: R_t = 42 cm; bottom: R_t = 8.5 cm.

the lack of flux enhancement in the localized spectrum cannot be explained because of changes in the profiles at high P_b.

Several possible complications in the data collected with the DNB on have been evaluated, including a possible decrease in DNB current from 190 to 280 ms, the possibility that the measured charge exchange flux might have been dominated by hydrogen impurities from the DNB, and counting losses of the channeltron detectors at high count rates. It is estimated that these effects working together might have caused a reduction in the localized flux during the two-beam phase of up to only ~30%. Since this uncertainty is smaller than the predicted increase in flux, it appears that the central fast ion density did not increase as expected from classical processes when the second beam was added to the first. At the same time, the line integrated spectra showed a flux increase which is consistent with classical confinement of the beam ions independently of P_b.

However, as indicated previously, the line integrated spectra were dominated by fast neutrals originating in the outer regions of the plasma, and thus they are not very sensitive to changes in the fast ion distribution function in the plasma core. Therefore, it seems possible that either some anomalous deposition process may have prevented the second beam from reaching the plasma centre, or a redistribution of the fast ions to a larger average radius may have taken place at the higher beam power.

The beams penetrated the plasma at a toroidal location close to the limiters. The deposition process might possibly have been affected by the higher con-

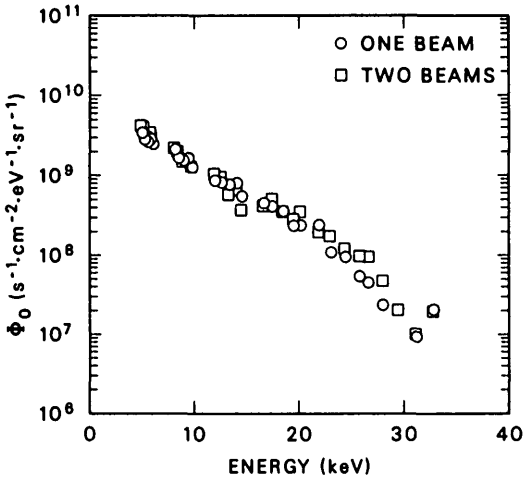

FIG. 17. Localized experimental spectra at R_t = 8.5 cm during one- and two-beam injection.

centration of impurities expected from recycling and sputtering during the two-beam phase. Two Monte Carlo simulations of the two-beam injection sequence were performed to investigate the effects of anomalous deposition on the resulting fast neutral spectra. In the first simulation, the local mean free paths of the incoming neutrals (λ) were artificially decreased by a factor of 2 throughout the plasma. In the other simulation, λ was decreased by a factor of 5 in the outermost four of the 20 radial shells. In both cases, the localized flux was predicted to be lower than in the straight simulations (except at $E \simeq E_{inj}$), but only by $\sim$15–20%. Since even these large changes in the deposition process could not account for the lack of enhancement in the localized flux with the second heating beam, it is unlikely that the experimental results could be explained on the basis of anomalous beam deposition. The same conclusion was reached by the TFR group in their experiment [16] during perpendicular injection.

The measured beam–plasma neutron yield decreased from 3.0×10^{10} neutrons$\cdot$s^{-1} at 190 ms to 2.1×10^{10} neutrons$\cdot$s^{-1} at 280 ms. The NEWORBX code predicts instead an *increase* from 2.3×10^{10} to 3.1×10^{10} neutrons$\cdot$s^{-1} at the same time points. Since only the first beam was doped with D^0, the experimentally measured decrease in the emission favours the interpretation that the beam ions spread away from the plasma centre after injection of the second beam. The reduction in the neutron yield could, however, also be attributed to a sizable decrease in the central deuterium target density upon injection of the second beam. Although a lower ratio of $n_D/(n_D + n_H)$ due to beam hydrogen fuelling was assumed in the simulation of the two-beam phase (0.75 versus 0.85 for the one-beam phase), the actual n_D dilution is not well known.

Evidence of a redistribution of the fast ions to a larger average radius during the internal disruptions in sawtoothing discharges was observed in ISX-B [17]. However, that effect cannot explain the data shown here, for the following reasons: the data were averaged over 6 ms, a time comparable to the sawtooth period ($\leq$10 ms); there was no sawtooth activity during the two-beam phase of the high-I_p discharge; the low-I_p discharge, which had no significant sawtooth activity, also showed little or no increase in the central fast neutral flux with the second heating beam.

4. CONCLUSIONS

Multi-angle, line integrated fast neutral spectra were collected during tangential injection in low-I_p discharges on the ISX-B. The spectra display marked differences, depending on the direction of injection (co or counter) and on the value of the plasma current. In all cases, the orbit following Monte Carlo simulation reproduces the spectra closely, indicating that classical theory describes adequately the beam ion thermalization process even in the low-I_p, large-orbit-width regime. Enhanced orbit losses at the lower I_p values were observed, but they were found to be consistent with the predictions of the present theory. Measurements of beam–plasma neutron emission support the conclusion that the beam ion behaviour on the ISX-B did not depart from that observed at higher I_p on other tokamaks. Furthermore, measured decay rates of the beam–plasma neutron production following beam turnoff show that the beam's slowing-down is classical within a 30% uncertainty, at least at energies close to E_{inj} and in the plasma core. That the slowing-down is classical may also be inferred from the good agreement between the experimental and predicted fast neutral spectra in both co- and counter-injection discharges, where the slowing-down is altered by differences in T_e and in the effects of the toroidal electric field. Beam additivity experiments indicated that, globally, the confinement of beam ions in the plasma volume was independent of the injected beam power in the ISX-B. However, local measurements of fast neutral spectra suggest that the fast ion density in the plasma core did not increase with P_b during tangential injection as expected from classical processes. The saturation of localized charge exchange flux with beam power does

not appear to depend strongly on the plasma current, nor on the injection geometry, since a similar saturation of central beam ion density with increasing beam power was also observed in TFR [16], where the beams were injected in a quasi-perpendicular direction. Together, the ISX-B and TFR results suggest that energetic beam ions may experience enhanced (non-classical) radial transport that carries them out of the plasma centre, even in discharges that do not exhibit perverse MHD behaviour such as fishbones [14]. Further work is clearly needed to verify the existence of such transport and its relation-ship to plasma conditions.

ACKNOWLEDGEMENTS

The authors are grateful to the members of the ISX-B operations and support staff for their contributions. This work was sponsored by the Office of Fusion Energy, US Department of Energy, under Contract No. DE-AC05-84OR21400 with Martin Marietta Energy Systems, Inc.

REFERENCES

[1] ZARNSTORFF, M.C., Bull. Am. Phys. Soc. **31** (9) (1986) 1383.
[2] BURRELL, K.H., STAMBAUGH, R.D., ANGEL, T.R., et al., Nucl. Fusion **23** (1983) 536.
[3] BOL, K., OKABAYASHI, M., FONCK, R., Nucl. Fusion **25** (1985) 1149.
[4] BERRY, L.A., BUSH, C.E., DUNLAP, J.L., et al., in Plasma Physics and Controlled Nuclear Fusion Research 1974 (Proc. 5th Int. Conf. Tokyo, 1974), Vol. 1, IAEA, Vienna (1975) 113.
[5] GOLDSTON, R.J., Nucl. Fusion **15** (1975) 651.
[6] CORDEY, J.G., GORBUNOV, E.P., HUGILL, J., et al., Nucl. Fusion **15** (1975) 441.
[7] VLASENKOV, V.S., KULYGIN, V.M., LEONOV, V.M., et al., in Plasma Physics and Controlled Nuclear Fusion Research 1976 (Proc. 6th Int. Conf. Berchtesgaden, 1976), Vol. 1, IAEA, Vienna (1977) 85.
[8] KAYE, S.M., GOLDSTON, R.J., Nucl. Fusion **25** (1985) 65.
[9] SWAIN, D.W., MURAKAMI, M., BATES, S.C., et al., Nucl. Fusion **21** (1981) 1409.
[10] EUBANK, H., GOLDSTON, R.J., ARUNASALAM, V., et al., in Plasma Physics and Controlled Nuclear Fusion Research 1978 (Proc. 7th Int. Conf. Innsbruck, 1978), Vol. 1, IAEA, Vienna (1979) 167.
[11] STRACHAN, J.D., COLESTOCK, P.L., DAVIS, S.L., et al., Nucl. Fusion **21** (1981) 67.
[12] TFR GROUP, Nucl. Fusion **23** (1983) 425.
[13] KAITA, R., GOLDSTON, R.J., BEIERSDORFER, P., et al., Nucl. Fusion **25** (1985) 939.
[14] McGUIRE, K., GOLDSTON, R.J., BELL, M., et al., Phys. Rev. Lett. **50** (1983) 891.
[15] WHITE, R.B., CHEN, L., ROMANELLI, F., HAY, R., Phys. Fluids **28** (1985) 278.
[16] TFR GROUP, in Controlled Fusion and Plasma Physics (Proc. 12th Eur. Conf. Budapest, 1985), Vol. 2, European Physical Society (1985) 308.
[17] CARNEVALI, A., An experimental investigation of fast ion confinement on the ISX-B tokamak, PhD Dissertation, University of Tennessee (1985).
[18] ISLER, R.C., WOOTTON, A.J., MURRAY, L.E., et al., Nucl. Fusion **26** (1986) 391.
[19] NEILSON, G.H., WOOTTON, A.J., BELL, J.D., et al., Nucl. Fusion **25** (1985) 825.
[20] LAZARUS, E.A., BELL, J.D., BUSH, C.E., et al., Nucl. Fusion **25** (1985) 135.
[21] MURAKAMI, M., BATES, S.C., BELL, J.D., et al., in Plasma Physics and Controlled Nuclear Fusion Research 1982 (Proc. 9th Int. Conf. Baltimore, 1982), Vol. 1, IAEA, Vienna (1983) 57.
[22] NEILSON, G.H., Charge Exchange Measurements of Ion Behavior in the ISX-B Tokamak, Rep. ORNL/TM-7333, Oak Ridge National Lab., Oak Ridge, TN (1980).
[23] SCOTT, S.D., An experimental investigation of magnetic field ripple effects on tokamak plasmas, PhD Dissertation, Massachusetts Institute of Technology, Cambridge, MA (1982).
[24] GOLDSTON, R.J. McCUNE, D.C., TOWNER, H.H., et al., J. Comput. Phys. **43** (1981) 61.
[25] FOWLER, R.H., ROME, J.A., Bull. Am. Phys. Soc. **25** 8 (1980) 849.
[26] BURRELL, K.H., J. Comput. Phys. **27** (1978) 88.
[27] McCRACKEN, G.M., STOTT, P.E., Nucl. Fusion **19** (1979) 889.
[28] BEHRISCH, R., in Tokamak Reactors for Breakeven (Proc. Int. School for Fusion Reactor Technology, Erice), Pergamon Press (1976) 37.
[29] THOMAS, D.M., Investigation of Edge Neutral Flux on the ISX-B Tokamak Using a Low-Energy Charge Exchange Analyzer, Rep. ORNL/TM-8671, Oak Ridge National Lab., Oak Ridge, TN (1983).
[30] DUNLAP, J.L., CARRERAS, B.A., PARÉ, V.K., et al., Phys. Rev. Lett. **48** (1982) 538.
[31] ROME, J.A., LYON, J.F., FOWLER, R.H., Using a Constants-of-Motion Space to Clarify Measurements Involving Energetic Ion Orbits in Tokamaks, Rep. ORNL/TM-7913, Oak Ridge National Lab., Oak Ridge, TN (1981).
[32] ISLER, R.C., MURRAY, L.E., CRUME, E.C., et al., Nucl. Fusion **23** (1983) 1017.
[33] ROME, J.A., McALEES, D.G., CALLEN, J.D., FOWLER, R.H., Nucl. Fusion **16** (1976) 55.
[34] FURTH, H.P., in Controlled Fusion and Plasma Physics (Proc. 6th Eur. Conf., Moscow 1973), Vol. 2, Joint Institute for Nuclear Research, Moscow (1973) 51.
[35] STRACHAN, J.D., GREK, B., HEIDBRINK, W., et al., Nucl. Fusion **25** (1985) 863.

(Manuscript received 28 April 1987
Final manuscript received 25 January 1988)